

# Design of Rigid-foldable Doubly-Curved Origami Tessellations Based on Trapezoidal Crease Patterns

Keyao Song<sup>1</sup>, Xiang Zhou<sup>1\*</sup>, Shixi Zang<sup>1</sup>, Hai Wang<sup>1</sup>, Zhong You<sup>2</sup>

<sup>1</sup> School of Aeronautics and Astronautics, Shanghai Jiao Tong University, No. 800 Dongchuan Road, Shanghai, 200240, China

<sup>2</sup> Department of Engineering Science, University of Oxford, Parks Road, Oxford, OX3 0PL, UK

## ABSTRACT

This paper presents a mathematical framework for the design of rigid-foldable doubly-curved origami tessellations based on trapezoidal crease patterns that can simultaneously fit two target surfaces with rotational symmetry about a common axis. The geometric parameters of the crease pattern and the folding angles of the target folded state are determined through a set of combined geometric and constraint equations. An algorithm to simulate the folding motion of the designed crease pattern is provided. Furthermore, the conditions and procedures to design folded ring structures that are both developable and flat-foldable and stacked folded structures consisting of two layers that can fold independently or compatibly are discussed. The proposed framework has potential applications in designing engineering doubly-curved structures such as deployable domes and folded cores for doubly-curved sandwich structures on the aircraft.

**Keywords:** doubly-curved origami structure, rigid-foldable, folded ring structure, stacked folded structure

---

\* Corresponding author, e-mail: xiangzhou@sjtu.edu.cn, telephone: +86 21 34207538, corresponding address: School of Aeronautics and Astronautics, No. 800 Dongchuan Road, Shanghai, 200240, China.

## 1. Introduction

Origami, an ancient art of folding a two-dimensional (2D) paper into a three-dimensional (3D) structure, has aroused considerable research interests from scientists and engineers in recent years due to some of the unique properties exhibited by the folded structures and consequently has inspired a wide spectrum of state-of-the-art applications ranging from deployable space solar panels (Zirbel *et al.* 2013) to medical stents (Kuribayashi *et al.* 2006), foldable electronic devices (Song *et al.* 2014; Tang *et al.* 2014; Zhang *et al.* 2015), lightweight sandwich folded cores (Heimbs 2013) and mechanical metamaterials (Schenk & Guest 2013; Wei *et al.* 2013; Silverberg *et al.* 2014; Waitukaitis *et al.* 2015; Zhou *et al.* 2016). In this context, a fundamental yet challenging issue is origami geometric design, which addresses the problem of how to create a crease pattern that folds into the desired 3D shape. Deriving parametric equations to describe the folding kinematics for a certain crease pattern is a commonly used approach by many researchers (Zakirov & Alekseev 2010; Wang & Chen 2011; Gattas *et al.* 2013). However, this approach suffers from vast mathematical complexity and often lacks flexibility and applicability in real circumstances. Lang (1996) proposed an origami design method, known as the tree method, which allows one to design hierarchical flat-folded origami silhouettes based on the concept of universal molecule. Tachi (2006) developed the first practical method for the construction of true 3D origami structures using edge- and vertex-tucking molecules. Later on, Tachi (2013) introduced a method to produce 3D origami structures from generalized Resch patterns that can approximate a given polyhedral surface. Zhou *et al.* (2015) developed a computer-based method, known as the vertex method, which can generate developable 3D origami structures between two singly-curved surfaces as well as simulate the unfolding process of the designed folded structure to the corresponding 2D crease pattern. More recently, Dudte *et al.* (2016) presented a numerical algorithm to generate developable origami tessellations that can yield approximations to given surfaces of constant or varying curvature. Despite these developments, designing developable origami tessellations to strictly fit between two doubly-curved target surfaces is still intractable.

In this paper, we present a mathematical framework for the generation of rigid-foldable 3D origami tessellations based on trapezoid-mesh crease patterns that can simultaneously fit two doubly-curved surfaces with rotational symmetry about a common axis. Specifically, the geometric parameters of

the trapezoidal crease pattern and the folding angles of the target 3D state whose outer and inner profiles are prescribed independently are determined by solving a set of mixed geometric and constraint equations. To facilitate the design process, an algorithm to simulate the interim folding sequence of the designed origami tessellation is provided. Furthermore, methods of designing developable and flat-foldable folded rings and stacked folded structures consisting of two layers that can fold independently or in a compatible manner are introduced. The potential applications of the proposed framework include but are not limited to creating deployable roofs or shelters in architecture and doubly-curved sandwich structures with folded cores on the aircraft.

The layout of the paper is as follows. First, the folding kinematics of the trapezoidal crease pattern is established, based on which a folding simulation algorithm and the fundamental inverse design theory are developed. Two design examples are provided. Then, the conditions and procedures to design folded ring structures and stacked folded structures are discussed. Finally, a brief summary concludes the paper.

## 2. Fundamental theory

### (a) Folding kinematics of the trapezoidal pattern

Figure 1a illustrates a single degree-4 vertex, where the valley and mountain creases are indicated by the blue and red lines, respectively, sector angles  $\angle AOB$  and  $\angle AOD$  are both equal to  $\varphi$  ( $\in [0, \pi/2]$ ), and creases  $OA$  and  $OC$  are collinear. The interim folded state of the degree-4 vertex is shown in figure 1b. Denote the dihedral angles along creases  $OA$ ,  $OB$ ,  $OC$  and  $OD$  by  $\theta_A$ ,  $\theta_B$ ,  $\theta_C$  and  $\theta_D$  ( $\in [0, \pi]$ ) and the angles formed by creases  $OA$  and  $OC$  and creases  $OB$  and  $OD$  by  $\eta_a$  and  $\eta_b$ , respectively. The following relationships can be obtained.

$$\theta_A = \theta_C, \quad (2.1)$$

$$\theta_B = \theta_D, \quad (2.2)$$

$$(1 + \cos^2 \varphi + \sin^2 \varphi \cos \theta_A)(1 + \cos^2 \varphi - \sin^2 \varphi \cos \theta_B) = 4 \cos^2 \varphi, \quad (2.3)$$

$$\cos \eta_a = \sin^2 \varphi \cos \theta_B - \cos^2 \varphi, \quad (2.4)$$

$$\cos \eta_b = \sin^2 \varphi \cos \theta_A + \cos^2 \varphi. \quad (2.5)$$

The detailed derivations of equations (2.1) to (2.5) are provided in the electronic supplementary material, section A.

Consider now a crease pattern comprising twelve trapezoidal facets shown in figure 2a, where all vertices locate on five auxiliary dashed lines  $\chi_{c1}$ ,  $\chi_{f1}$ ,  $\chi_{c2}$ ,  $\chi_{f2}$  and  $\chi_{c3}$  that intersect at point  $O$ , the angle formed by any two adjacent  $\chi$  lines equals  $\alpha_0$  and the creases and boundary lines (i.e. the gray lines) extending between any two adjacent  $\chi$  lines are all parallel to each other. For clarity, we refer herein the creases or boundary lines extending along the  $\chi$  lines as the radial creases or boundary lines and the rest as the circumferential creases or boundary lines. Any two adjacent circumferential creases or boundary lines are symmetrical about the  $\chi$  line passing through their common point. Denote the length of line segment  $C_{1,k}C_{1,k+1}$  by  $a_{ck}$ , where  $k = 1, 2, 3$ , the length of line segment  $F_{1,k}F_{1,k+1}$  by  $a_{fk}$ , where  $k = 1, 2, 3$ , the length of line segment  $C_{1,k}F_{1,k}$  by  $b_k$ , where  $k = 1, \dots, 4$ , the acute angle formed by line segment  $C_{11}F_{11}$  and line  $\chi_{c1}$  by  $\varphi_c$ , and the acute angle formed by line segment  $C_{11}F_{11}$  and line  $\chi_{fk}$  by  $\varphi_f$ . The following simple geometric relationships can be obtained.

$$\varphi_c - \varphi_f = \alpha_0, \quad (2.6)$$

$$\frac{a_{ck}}{a_{fk}} = \frac{\sin \varphi_f}{\sin \varphi_c}, k = 1, 2, 3, \quad (2.7)$$

$$b_k = b_1 + \frac{\sin \alpha_0}{\sin \varphi_f} \sum_{i=1}^{k-1} a_{ci}, k = 2, 3, 4. \quad (2.8)$$

The interim folded state of the crease pattern is illustrated in figure 2b. Each internal vertex of the crease pattern is a degree-4 vertex shown in figure 1. According to equations (2.1) to (2.3), all of the dihedral angles along the collinear radial creases and all of those along the circumferential creases are equal. Due to symmetry, the dihedral angles along the creases on line  $\chi_{f1}$  are equal to those along the creases on line  $\chi_{f2}$ . Hence, we denote the dihedral angles along the radial creases on lines  $\chi_{f1}$  and  $\chi_{f2}$  by  $\theta_{fa}$ , those along the radial creases on line  $\chi_{c2}$  by  $\theta_{ca}$  and those along the circumferential creases by  $\theta_b$ . Applying equation (2.3) to each internal vertex, the following two equations can be obtained.

$$(1 + \cos^2 \varphi_c + \sin^2 \varphi_c \cos \theta_{ca})(1 + \cos^2 \varphi_c - \sin^2 \varphi_c \cos \theta_b) = 4 \cos^2 \varphi_c, \quad (2.9)$$

$$(1 + \cos^2 \varphi_f + \sin^2 \varphi_f \cos \theta_{fa})(1 + \cos^2 \varphi_f - \sin^2 \varphi_f \cos \theta_b) = 4 \cos^2 \varphi_f. \quad (2.10)$$

Note that there are total three independent geometric parameters  $\theta_{ca}$ ,  $\theta_{fa}$  and  $\theta_b$  governed by

two kinematics equations. Therefore, the crease pattern shown in figure 2 has single degree-of-freedom (DOF) of rigid folding motion. Besides, when  $\theta_b$  becomes zero, both  $\theta_{ca}$  and  $\theta_{fa}$  reach zero according to equations (2.9) and (2.10), indicating that the crease pattern is flat-foldable. The same conclusions are applicable to a general case with any number of  $\chi$  lines and any number of vertices along the  $\chi$  lines.

*(b) Motion simulation of the trapezoidal pattern*

According to equation (2.4) and the relationships among the dihedral angles discussed above, the angles formed by the radial creases at all internal vertices that locate on the  $\chi_f$  lines (subsequently referred as the F-type vertices) are equal. So are those formed by the radial creases or boundary lines at all vertices that locate on the  $\chi_c$  lines (subsequently referred as the C-type vertices). The similar relationships can be found for the angles formed by the circumferential creases or boundary lines. Hence, we denote the angles formed by the radial creases at the F-type vertices by  $\eta_{fa}$ , those by the radial creases or boundary lines at the C-type vertices by  $\eta_{ca}$  and the circumferential counterparts by  $\eta_{fb}$  and  $\eta_{cb}$ , respectively. According to equations (2.4) and (2.5), they can be determined as

$$\cos \eta_{ca} = \sin^2 \varphi_c \cos \theta_b - \cos^2 \varphi_c, \quad (2.11)$$

$$\cos \eta_{cb} = \sin^2 \varphi_c \cos \theta_{ca} + \cos^2 \varphi_c, \quad (2.12)$$

$$\cos \eta_{fa} = \sin^2 \varphi_f \cos \theta_b - \cos^2 \varphi_f, \quad (2.13)$$

$$\cos \eta_{fb} = \sin^2 \varphi_f \cos \theta_{fa} + \cos^2 \varphi_f. \quad (2.14)$$

To derive the positions of the vertices, we define a cylindrical coordinate system (see figure 2b) whose  $z$ -axis is perpendicular to the plane defined by the circumferential boundary lines passing through  $C_{i,1}$  and  $F_{j,1}$ , where  $i = 1, 2, 3$  and  $j = 1, 2$ ,  $r$ -axis passes through  $C_{11}$  and origin  $O$  has equal distances to  $C_{i,1}$ ,  $i = 1, 2, 3$ . Denote the projected lengths of line segments  $C_{11}C_{12}$ ,  $C_{12}C_{13}$  and  $C_{13}C_{14}$  on the  $z$ -axis by  $h_1$ ,  $h_2$  and  $h_3$ , respectively. They can be determined as

$$h_k = a_{ck} \cos(\eta_{ca}/2), k = 1, 2, 3. \quad (2.15)$$

The sector angle  $\alpha$ , defined by the angle formed by line segments  $OF_{k,1}$  and  $OC_{k,1}$  or  $OC_{k+1,1}$ ,  $k = 1, 2$ , is given by

$$\alpha = (\eta_{cb} - \eta_{fb})/2. \quad (2.16)$$

Finally, for a general trapezoidal crease pattern containing  $m \times n$  C-type vertices and  $(m - 1) \times n$  F-type vertices, the coordinates of the C-type vertices are obtained as

$$r_{i,j}^c = \frac{b_j \sin(\eta_{fb}/2)}{\sin \alpha}, i = 1, \dots, m, j = 1, \dots, n, \quad (2.17)$$

$$\theta_{i,j}^c = 2(i - 1)\alpha, i = 1, \dots, m, j = 1, \dots, n, \quad (2.18)$$

$$z_{i,1}^c = 0, i = 1, \dots, m \quad (2.19)$$

$$z_{i,j}^c = \sum_{k=1}^{j-1} (-1)^k h_k, i = 1, \dots, m, j = 2, \dots, n, \quad (2.20)$$

and those of the F-type vertices as

$$r_{i,j}^f = \frac{b_j \sin(\eta_{cb}/2)}{\sin \alpha}, i = 1, \dots, m - 1, j = 1, \dots, n, \quad (2.21)$$

$$\theta_{i,j}^f = (2i - 1)\alpha, i = 1, \dots, m - 1, j = 1, \dots, n, \quad (2.22)$$

$$z_{i,j}^f = z_{i,j}^c, i = 1, \dots, m - 1, j = 1, \dots, n. \quad (2.23)$$

The algorithm to simulate the folding motion of the trapezoidal pattern is as follows. First, select one of the three dihedral angles as the control parameter. Then, solve the other two dihedral angles through equations (2.9) and (2.10). Next,  $\eta_{ca}$ ,  $\eta_{fa}$ ,  $\eta_{cb}$  and  $\eta_{fb}$  are determined through equations (2.11) to (2.14). Finally, the coordinates of all the vertices are obtained using equations (2.17) to (2.23), with which the current interim folded state is determined.

### (c) Inverse design algorithm

The folded structure of the trapezoidal pattern, as illustrated in figure 2b, has rotational symmetry about the  $z$ -axis. Hence, projecting all the vertices and creases onto the  $r$ - $z$  plane yields a superimposed 2D pattern shown in figure 3. It is noted that the outer and inner cross-sectional profiles of the folded structure are determined by the F-type vertices with odd radial indices, i.e.  $F_{i,j}$ ,  $i = 1, \dots, m - 1$ ,  $j = \text{odd}$  and the C-type vertices with even radial indices, i.e.  $C_{i,j}$ ,  $i = 1, \dots, m$ ,  $j = \text{even}$ , respectively. Given two non-intersecting doubly-curved surfaces with rotational symmetry about the  $z$ -axis whose cross-section equations in the  $r$ - $z$  plane are given by  $z = f_{out}(r)$  and  $z = f_{in}(r)$ , respectively, in order for the folded structure to fit into the interspace

between these surfaces, the following constraints need to be satisfied for arbitrary  $i$ .

$$\tilde{z}_{i,2j-1}^f = f_{out}(r_{i,2j-1}^f), j = 1, \dots, [(n+1)/2], \quad (2.24)$$

$$\tilde{z}_{i,2j}^c = f_{in}(r_{i,2j}^c), j = 1, \dots, [n/2], \quad (2.25)$$

where  $[\zeta]$  means taking the integer part of a real number  $\zeta$ , and  $\tilde{z}_{i,j}^c$  and  $\tilde{z}_{i,j}^f$  are the  $z$ -coordinates of the C-type and F-type vertices of the folded structure with an offset distance  $h_0$  along the  $z$ -axis, respectively, i.e.

$$\tilde{z}_{i,j}^c = \tilde{z}_{i,j}^f = z_{i,j}^c + h_0, i = 1, \dots, m, j = 1, \dots, n. \quad (2.26)$$

Furthermore, given that the total height of the folded structure in  $z$ -direction is  $H_z$  and the circumferential span is  $\theta_s$  ( $\in [0, 2\pi]$ ), the following constraints hold for arbitrary  $i$

$$H_z = \begin{cases} \tilde{z}_{i,1}^c - \tilde{z}_{i,n}^c, & \text{if } n = \text{even} \\ \tilde{z}_{i,1}^c - \tilde{z}_{i,n-1}^c, & \text{if } n = \text{odd} \end{cases}, \quad (2.27)$$

$$\theta_s = \theta_{m,j}^c - \theta_{1,j}^c = 2(m-1)\alpha. \quad (2.28)$$

To design a folded structure,  $\alpha$  can be determined independently from equation (2.28) where it is assumed that  $m$  and  $n$  are design inputs. Then, equations (2.24), (2.25) and (2.27) along with equations (2.9) to (2.14) and (2.16) can be solved together for parameters  $\varphi_c$ ,  $\varphi_f$ ,  $a_{ci}$ ,  $b_1$ ,  $\theta_{ca}$ ,  $\theta_{fa}$ ,  $\theta_b$ ,  $\eta_{ca}$ ,  $\eta_{cb}$ ,  $\eta_{fa}$ ,  $\eta_{fb}$  and  $h_0$ , where  $i = 1, \dots, n-1$ . Note that the total number of equations and unknowns are counted as  $n+8$  and  $n+10$ , respectively. Hence, two out of the  $n+10$  parameters need to be chosen as the control parameters so that the rest can be uniquely determined by the equations. In other words, the design DOF is two. Once these parameters are solved, the rest of the geometric parameters of the plane crease pattern can be determined using equations (2.6) to (2.8) and the resulting folded structure determined by equations (2.17) to (2.23).

#### (d) Examples

To demonstrate the inverse design process discussed above, two examples are provided below. In the first example, the outer and inner cross-sectional profiles are given by

$$z = f_{out}(r) = 0.0015r^2 + 450, \quad (2.29)$$

and

$$z = f_{in}(r) = 0.0021r^2 + 440, \quad (2.30)$$

respectively. The design inputs  $m$ ,  $n$ ,  $H_z$  and  $\theta_s$  are taken as 16, 21, 100 mm and  $3\pi/2$  rad, respectively.  $h_0$  and  $\varphi_c$  are chosen as the control parameters whose values are taken as 445 mm and  $\pi/3$  rad, respectively. The calculated parameters are listed in table 1. The resulting folded geometry and the corresponding 2D crease pattern are shown in figure 4. An animation of the folding motion of this example is provided in electronic supplementary material, movie S1.

The outer and inner cross-sectional profiles of the second example are determined as

$$z = f_{out}(r) = n_1 - \sqrt{n_1^2 - \frac{n_1^2}{m_1^2}(r - m_1 + 40)^2}, \quad (2.31)$$

and

$$z = f_{in}(r) = n_1 - \sqrt{n_2^2 - \frac{n_2^2}{m_2^2}(r - m_1 + 40)^2}, \quad (2.32)$$

respectively, where  $m_1$ ,  $n_1$ ,  $m_2$  and  $n_2$  are 580, 300, 575, 278, respectively. The design inputs  $m$ ,  $n$ ,  $H_z$  and  $\theta_s$  are the same as the first example. Again,  $h_0$  and  $\varphi_c$  are taken as the control parameters and their values are taken as 140 mm and  $\pi/3$  rad, respectively. The calculated parameters and resulting folded structure are shown in table 2 and figure 5, respectively. An animation of the folding motion is provided in electronic supplementary material, movie S2. It is noted that in both examples the designed folded structures strictly fit between the given outer and inner profiles (figures 4b and 5b), indicating the validity of the proposed design theory.

### 3. Discussion

#### (a) Developable and flat-foldable ring design

For some practical applications, it is desirable to design a folded structure that can not only fit between the given surfaces but at the same time form a closed ring by itself. In other words, it is desired that the opposite edges in the  $\theta$  direction of the folded structure meet each other, which can be achieved by making  $\theta_s$  in equation (2.28) equal  $2\pi$ , i.e.

$$(m - 1)\alpha = \pi. \quad (3.1)$$

If it is further required that the designed folded structure satisfying equation (3.1) is both developable and flat-foldable for the ease of assembly, storage or transportation, the following conditions must be satisfied.



$$\varphi_c > \frac{\pi}{4}, \varphi_c + \varphi_f > \frac{\pi}{2}, \quad (3.2)$$

and

$$\cos \theta_b = \frac{\sin 2\varphi_f (1 + \cos^2 \varphi_c) - \sin 2\varphi_c (1 + \cos^2 \varphi_f)}{\sin 2\varphi_f \sin^2 \varphi_c - \sin 2\varphi_c \sin^2 \varphi_f}. \quad (3.3)$$

The detailed derivations of these conditions are provided in the electronic supplementary material, section B. A physical illustration of how these conditions work is provided in figure 4, where the solid, dashed and dotted lines correspond to three cases in which  $\varphi_c = 70^\circ$  and  $\varphi_f = 60^\circ$ ,  $\varphi_c = 50^\circ$  and  $\varphi_f = 40^\circ$ , and  $\varphi_c = 30^\circ$  and  $\varphi_f = 20^\circ$ , respectively. It is shown that there exists a maximum value for  $\alpha$ , denoted by  $\alpha_{max}$ , only when inequality (3.2) is strictly satisfied, i.e. the solid line. Under this circumstance, when  $\alpha$  of the designed folded structure locates either left or right to the peak, the folded structure is either flat-foldable but not developable or the other way round due to the penetration of the opposite edges in the  $\theta$  direction during folding or unfolding which is physically prohibited. Only when  $\alpha$  of the designed folded structure is equal to  $\alpha_{max}$  can it be both developable and flat-foldable. Equation (3.3) ensures that  $\theta_b$  of the designed structure corresponds to the peak position of  $\alpha$  on the curve. If inequality (3.2) is not satisfied (e.g. the dashed and dotted lines),  $\alpha$  increases monotonically with  $\theta_b$ , indicating that the designed folded structure is always flat-foldable but not developable.

The algorithm to design a developable and flat-foldable self-closed folded ring is as follows. First,  $\alpha$  is determined through equation (3.1). Then, equations (2.9) to (2.14), (2.16), (2.24), (2.25), (2.27) and (3.3) are solved together to obtain parameters  $\varphi_c$ ,  $\varphi_f$ ,  $a_{ci}$ ,  $b_1$ ,  $\theta_{ca}$ ,  $\theta_{fa}$ ,  $\theta_b$ ,  $\eta_{ca}$ ,  $\eta_{cb}$ ,  $\eta_{fa}$ ,  $\eta_{fb}$  and  $h_0$ , where  $i = 1, \dots, n-1$ . Note that the total number of equations and unknowns are  $n+9$  and  $n+10$ , respectively. Hence, the design DOF is now reduced to one. Due to inequality (3.2), it is convenient to choose  $\varphi_c$  as the control parameter which is set to be larger than  $\pi/4$  rad. Once the other parameters are solved, one ought to check back if inequality (3.2) is satisfied. Alternatively, one may specify both  $\varphi_c$  and  $h_0$  and solve the remaining parameters without equation (3.3) in the first step. Next, keep  $h_0$  unchanged as the sole control parameter and solve the rest parameters including  $\varphi_c$  with equation (3.3) included. In this second step, the specified value for  $\varphi_c$  and the solutions of the other parameters obtained in the first step can be used as the initial guesses for solutions of the non-linear equation system. Usually, as long as  $m$  is large

enough and  $\varphi_c$  is set to be well above  $\pi/4$  rad, inequality (3.2) can always be satisfied.

A design example is given here in which  $m = n = 21$ ,  $H_z = 100$  mm,  $\theta_s = 2\pi$  rad, and the outer and inner cross-sectional profiles of the target surfaces are

$$z = f_{out}(r) = 450 \sqrt{1 - \frac{r^2}{580^2}}, \quad (3.4)$$

and

$$z = f_{in}(r) = 440 \sqrt{1 - \frac{r^2}{480^2}}, \quad (3.5)$$

respectively. First, we use  $h_0$  and  $\varphi_c$  as the control parameters whose values are taken as 445 mm and  $\pi/3$  rad, respectively, and the rest parameters are solved using the inverse design algorithm discussed in section 2(c). Then,  $h_0$  is taken as the sole control parameter, and the remaining parameters including  $\varphi_c$  are solved with equation (3.3). The obtained parameters are listed in table 3. The graphic results are shown in figure 7. An animation of the folding motion of the structure is provided in electronic supplementary material, movie S3. Note that the designed folded structure forms a complete ring (figure 7a) and strictly fits between the inner and outer profiles (figure 7b). Moreover, the total circumferential span of the folded structure is always smaller than  $2\pi$  during the entire folding range (figure 7d), indicating that the designed folded structure is both developable and flat-foldable.

Consider another example in which the prescribed outer and inner surfaces have negative and positive Gaussian curvatures, respectively, whose cross-sectional profiles are determined as

$$z = f_{out}(r) = 300 - \sqrt{300^2 - \frac{300^2}{580^2}(r - 540)^2}, \quad (3.6)$$

and

$$z = f_{in}(r) = -0.0038(r + 80)^2 + 190, \quad (3.7)$$

respectively. The design inputs  $m$ ,  $n$ ,  $H_z$  and  $\theta_s$  are the same as the previous example, and the control parameter  $h_0$  is taken as 160 mm. The obtained parameters are summarized in table 4, the graphic results are illustrated in figure 8, and an animation of the folding motion of the structure is provided in electronic supplementary material, movie S4. Again, the designed ring structure

successfully satisfies both the prescribed geometries (figure 8b) and the developable and flat-foldable requirement (figure 8d).

(b) *Stacked design*

The design algorithm discussed above can be generalized to design stacked folded structures consisting of multiple folded layers. For simplicity, only the two-layer configuration is discussed here, as shown in figure 9. In the sequel, we refer the bottom and top layers as layer 1 and 2, respectively. In each individual layer, equations (2.6) to (2.23) still hold except that equation (2.20) in layer 2 is modified as

$$z_{i,j}^c = \sum_{k=1}^{j-1} (-1)^{k+1} h_k, i = 1, \dots, m, j = 2, \dots, n, \quad (3.8)$$

due to the reversed mountain-valley assignment for the creases in layer 2. It is noted that the outer and inner profiles of the folded structure are determined by the F-type vertices with even radial indices in the top layer and the C-type vertices with even radial indices in the bottom layer, respectively. Therefore, given two non-intersecting surfaces with rotational symmetry about the  $z$ -axis whose cross-section equations in the  $r$ - $z$  plane are given by  $z = f_{out}(r)$  and  $z = f_{in}(r)$ , respectively, the following constraints need to be satisfied for arbitrary  $i$

$$\tilde{z}_{i,2j}^{f,2} = f_{out}(r_{i,2j}^{f,2}), j = 1, \dots, [n/2], \quad (3.9)$$

$$\tilde{z}_{i,2j}^{c,1} = f_{in}(r_{i,2j}^{c,1}), j = 1, \dots, [n/2]. \quad (3.10)$$

where the superscripts 1 and 2 denote the layer numbers, and

$$\tilde{z}_{i,j}^{c,1} = \tilde{z}_{i,j}^{f,1} = z_{i,j}^{c,1} + h_0^1, i = 1, \dots, m, j = 1, \dots, n, \quad (3.11)$$

$$\tilde{z}_{i,j}^{c,2} = \tilde{z}_{i,j}^{f,2} = z_{i,j}^{c,2} + h_0^2, i = 1, \dots, m, j = 1, \dots, n. \quad (3.12)$$

On the interface between the two layers, the C- and F-type vertices with odd radial indices in layer 2 should coincide with those in layer 1, respectively. Under this requirement, the following relationships can be obtained according to figure 2b.

$$\eta_{cb}^1 = \eta_{cb}^2, \quad (3.13)$$

$$\eta_{fb}^1 = \eta_{fb}^2, \quad (3.14)$$

and

$$\alpha^1 = \alpha^2. \quad (3.15)$$

Due to equation (2.16), two of the three equations are independent. Equation (3.15) ensures that the position constraints in the  $\theta$  direction for both C- and F-type vertices on the interface are satisfied. For the C-type vertices, the position constraints the  $r$  and  $z$  directions are given by

$$r_{i,2j-1}^{c,1} = r_{i,2j-1}^{c,2}, j = 1, \dots, [(n+1)/2], \quad (3.16)$$

$$\tilde{z}_{i,2j-1}^{c,1} = \tilde{z}_{i,2j-1}^{c,2}, j = 1, \dots, [(n+1)/2]. \quad (3.17)$$

Substituting equations (2.17), (3.14) and (3.15) into equation (3.16) yields

$$b_j^1 = b_j^2, j = \text{odd}. \quad (3.18)$$

Considering equations (2.21), (3.13), (3.15) and (3.18) together and due to equation (2.23), the constraints in the  $r$  and  $z$  directions for the F-type vertices on the interface are automatically satisfied. Furthermore, given the total height of the stacked folded structure in  $z$ -direction  $H_z$  and the circumferential span  $\theta_s$  ( $\in [0, 2\pi]$ ), the following constraints hold for arbitrary  $i$

$$H_z = \begin{cases} \tilde{z}_{i,2}^{c,2} - \tilde{z}_{i,n}^{c,1}, & \text{if } n = \text{even} \\ \tilde{z}_{i,1}^{c,2} - \tilde{z}_{i,n-1}^{c,1}, & \text{if } n = \text{odd} \end{cases}, \quad (3.19)$$

$$\theta_s = 2(m-1)\alpha^1 = 2(m-1)\alpha^2. \quad (3.20)$$

To design a stacked folded structure,  $\alpha^1$  and  $\alpha^2$  can be determined directly from equation (3.20). Then, equations (2.9) to (2.14) and (2.16) for both layers along with constraint equations (3.9), (3.10) and (3.13), (3.16), (3.17) and (3.19) can be solve together for parameters  $\varphi_c^k$ ,  $\varphi_f^k$ ,  $a_{ci}^k$ ,  $b_1^k$ ,  $\theta_{ca}^k$ ,  $\theta_{fa}^k$ ,  $\theta_b^k$ ,  $\eta_{ca}^k$ ,  $\eta_{cb}^k$ ,  $\eta_{fa}^k$ ,  $\eta_{fb}^k$  and  $h_0^k$ , where  $k = 1, 2$  and  $i = 1, \dots, n-1$ . Note that the total numbers of equations and unknowns in the equation system are  $2(n+8)$  and  $2(n+10)$ , respectively. Therefore, the design DOF for the two-layer configuration is four.

If a stacked folded ring structure is to be designed, one needs simply to set  $\theta_s$  in equation (3.20) to  $2\pi$ . If it is further required that each layer in the structure is both flat-foldable and developable, conditions given in inequality (3.2) and equation (3.3) should be satisfied by each layer. Adding equation (3.3) for each layer into the overall equation system of the stacked structure reduces the total design DOF from four to two. The selection of control parameters is similar to the single-layered ring design discussed in section 3a.

For certain applications, it is desirable that both layers of the designed stacked folded structure can fold or unfold together in a compatible manner. To achieve this, the following condition needs to be satisfied.

$$\varphi_c^1 = \varphi_c^2. \quad (3.21)$$

The detailed derivation of equation (3.21) is provided in the electronic supplementary material, section C. In this context, when a developable and flat-foldable stacked ring structure is to be designed, due to the compatible folding condition enforced by equation (3.21), the entire structure is developable and flat-foldable as long as inequality (3.2) and equation (3.3) are satisfied by any one of the constituent layers. Therefore, the total design DOF remains two. As a rule of thumb,  $h_0^1$  and  $\varphi_c^1$  are the robust choices for the control parameters.

We finalize this section with a design example for a developable, flat-foldable and compatibly-foldable stacked ring structure, where  $m = 19$ ,  $n = 21$ ,  $H_z = 117$  mm,  $\theta_s = 2\pi$  rad, and the outer and inner cross-sectional profiles of the target surfaces are given by

$$z = f_{out}(r) = 480 \sqrt{1 - \frac{r^2}{650^2}}, \quad (3.22)$$

and

$$z = f_{in}(r) = 460 \sqrt{1 - \frac{r^2}{550^2}}, \quad (3.23)$$

respectively. The control parameters are  $h_0^1$  and  $\varphi_c^1$  and they are taken as 470 mm and  $\pi/3$  rad, respectively. The calculated parameters are listed in tables 5 and 6. The graphic results are plotted in figure 10. Animations of the folding motion of the 3D structure and the cross-sectional profile change are provided in electronic supplementary material, movies S5 and movie S6, respectively. The results suggest that the designed stacked ring structure strictly fits between the inner and outer profiles (figure 10b) and is developable and flat-foldable (figure 10e) and the two layers do not separate throughout the folding motion (movie S6).

#### 4. Summary and final remarks

In this paper, a mathematical framework for the design of rigid-foldable doubly-curved origami tessellations that can fit between two doubly-curved target surfaces with rotational symmetry about

a common axis has been established. Under the framework, an algorithm to simulate the folding motion of the designed origami structure is provided, and specific conditions for the design of doubly-curved folded ring structures that are developable and flat-foldable and stacked folded structures whose constituent layers can fold independently or in a compatible manner are identified. The validity and versatility of the proposed framework were demonstrated by several design examples and paper models. This study paves the way towards various potential engineering applications. For example, the developable and flat-foldable ring design with 1-DOF rigid folding motion are particularly useful for designing retractable domes or portable shelters requiring minimum driving systems. When manufactured with composite materials, such as CFRP and Kevlar prepregs, the doubly-curved folded structures can help guide the development of lightweight folded cores for doubly-curved sandwich structures on the aircraft, such as fairing and fuselage. Moreover, the stacked folded structures with compatibly foldable layers may lead to new doubly-curved tunable metamaterial designs with intriguing properties. The main limitation of the current work is that the designed folded structures can only fit between two doubly-curved surfaces with rotational symmetry about a common axis. Chopping off the parallel condition for the creases and boundary lines extending between any two adjacent  $\chi$  lines in figure 2a and introducing proper diagonal creases to the general quadrilateral facets is a potential direction to overcome this limitation, which will be considered in our future work.

#### **Data accessibility**

The electronic supplementary materials supporting this article are available via <http://rspa.royalsocietypublishing.org>.

#### **Competing interests**

We have no competing interests.

#### **Authors' contributions**

K.S. derived some of the equations, wrote computer programs for the examples and made the physical models; X.Z. designed the study, derived some of the equations and wrote the paper; S.Z. derived some of the equations; H.W. coordinated the study and commented on the paper; Z.Y.

conceived of the study and commented on the paper. All authors gave final approval for publication.

### Acknowledgements

X.Z. wishes to acknowledge the financial support from National Natural Science Foundation of China (No. 51408357).

### Funding

X.Z. is funded by National Science Foundation of China (No. 51408357).

### References

Dudte, L. H., Vouga, E., Tachi, T. & Mahadevan, L. 2016 Programming curvature using origami tessellations. *Nat. Mat.* **15**, 583-589. (doi: 10.1038/NMAT4540)

Gattas, J. M., Wu, W. & You, Z. 2013 Miura-base rigid origami: parameterizations of first-level derivative and piecewise geometries. *J. Mech. Des.* **135**, 111011. (doi: 10.1115/1.4025380)

Heimbs, S. 2013 Foldcore sandwich structures and their impact behaviour: an overview. In *Dynamic Failure of Composite and Sandwich Structures*, pp. 491-544. Netherlands: Springer.

Kuribayashi, K., Tsuchiya, K., You, Z., Tomus, D., Umemoto, M., Ito, T. & Sasaki, M. 2006 Self-deployable origami stent grafts as a biomedical application of Ni-rich TiNi shape memory alloy foil. *Mat. Sci. Eng. A* **419**, 131-137. (doi: 10.1016/j.msea.2005.12.016)

Lang, R. J. 1996 A computational algorithm for origami design. In *Proceedings of the twelfth annual symposium on computational geometry*, pp. 98-105. New York, NY: ACM. (doi: 10.1145/237218.237249)

Schenk, M. & Guest, S. D. 2013 Geometry of Miura-folded metamaterials. *P. Natl. Acad. Sci. USA.* **110**, 3276-3281. (doi: 10.1073/pnas.1217998110)

Silverberg, J. L., Evans, A. A., McLeod, L., Hayward, R. C., Hull, T., Santangelo, C. D. & Cohen, I. 2014 Using origami design principles to fold reprogrammable mechanical metamaterials. *Science* **345**, 647-650. (doi: 10.1126/science.1252876)

Song, Z., Ma, T., Tang, R., Cheng, Q., Wang, X., Krishnaraju, D., Panat, R., Chan, C. K., Yu, H. & Jiang, H. 2014 Origami lithium-ion batteries. *Nat. Commun.* **5**. (doi: 10.1038/ncomms4140)

Tachi, T. 2006 3D origami design based on tucking molecule. In *Origami<sup>4</sup>* (ed. R. J. Lang), pp. 259-272. Natick, MA: A. K. Peters.

Tachi, T. 2013 Designing freeform origami tessellations by generalizing Resch's pattern. *J. Mech. Des.* **135**, 111006. (doi: 10.1115/1.4025389)

Tang, R., Huang, H., Tu, H., Liang, H., Liang, M., Song, Z., Xu, Y., Jiang, H. & Yu, H. 2014 Origami-enabled deformable silicon solar cells. *Appl. Phys. Lett.* **104**, 083501. (doi: 10.1063/1.4866145)

Waitukaitis, S., Menaut, R., Chen, B. G. G., & van Hecke, M. 2015 Origami multistability: From single vertices to metasheets. *Phys. Rev. Lett.* **114**, 055503. (doi: 10.1103/PhysRevLett.114.055503)

Wang, K. & Chen, Y. 2011 Folding a patterned cylinder by rigid origami. In *Origami<sup>5</sup>* (ed. P. Wang-Iverson, R. J. Lang & M. Yim), pp. 29-38. Boca Raton, FL: CRC Peters.

Wei, Z. Y., Guo, Z. V., Dudte, L., Liang, H. Y. & Mahadevan, L. 2013 Geometric mechanics of periodic pleated origami. *Phys. Rev. Lett.* **110**, 215501. (doi: 10.1103/PhysRevLett.110.215501)

Zakirov, I. M. & Alekseev, K. A. 2010 Design of a wedge-shaped folded structure. *J. Mach. Manufact. Reliab.* **39**, 412-417. (doi: 10.3103/S105261881005002X)

Zhang, Y., Huang, Y. & Rogers, J. A. 2015 Mechanics of stretchable batteries and supercapacitors.



*Current Opinion in Solid State and Materials Science* **19**, 190-199. (doi: 10.1016/j.cossms.2015.01.002)

Zhou, X., Wang, H. & You, Z. 2015 Design of three-dimensional origami structures based on a vertex approach. *Proc. R. Soc. A* **471**, 20150407. (doi: 10.1098/rspa.2015.0407)

Zhou, X., Zhang, S. & You, Z. 2016 Origami mechanical metamaterials based on the Miura-derivative fold patterns. *Proc. R. Soc. A* **472**, 20160361. (doi: 10.1098/rspa.2016.0361)

Zirbel, S. A., Lang, R. J., Thomson, M. W., Sigel, D. A., Walkemeyer, P. E., Trease, B. P., Magleby S. P. & Howell, L. L. 2013 Accommodating thickness in origami-based deployable arrays. *J. Mech. Des.* **135**, 111005. (doi: 10.1115/1.4025372)

### List of figures

- Figure 1 (a) A single degree-4 vertex; (b) The interim folded state of the degree-4 vertex.
- Figure 2 (a) A trapezoidal crease pattern comprising twelve trapezoidal facets; (b) The interim folded state of the trapezoidal crease pattern.
- Figure 3 The cross-sectional view in the  $r$ - $z$  plane of the folded state in figure 2b, in which all the vertices and creases are projected onto the same  $r$ - $z$  plane.
- Figure 4 (a) The resulting target folded structure of the first example; (b) The cross-sectional view of the target folded structure in which the red lines indicate the given outer and inner profiles; (c) The corresponding 2D crease pattern; (d) A paper model of the designed folded structure.
- Figure 5 (a) The resulting target folded structure of the second example; (b) The cross-sectional view of the target folded structure in which the red lines indicate the given outer and inner profiles; (c) The corresponding 2D crease pattern; (d) A paper model of the designed folded structure.
- Figure 6 Explanation of the developable and flat-foldable condition of the ring design.
- Figure 7 (a) The resulting target folded structure of the first developable and flat-foldable ring design example; (b) The cross-sectional view of the target folded structure in which the red lines indicate the given outer and inner profiles; (c) The corresponding 2D crease pattern; (d) The  $\theta_s$  versus  $\theta_b$  curve where the blue circle indicates the designed state; (e) A paper model of the designed folded structure.
- Figure 8 (a) The resulting target folded structure of the second developable and flat-foldable ring design example; (b) The cross-sectional view of the target folded structure in which the red lines indicate the given outer and inner profiles; (c) The corresponding 2D crease pattern; (d) The  $\theta_s$  versus  $\theta_b$  curve where the blue circle indicates the designed state; (e) A paper model of the designed folded structure.
- Figure 9 The cross-sectional profile of a two-layer configuration viewed in the  $r$ - $z$  plane.
- Figure 10 (a) The resulting target folded structure of the stacked ring design example; (b)

The cross-sectional view of the target folded structure in which the red lines indicate the given outer and inner profiles and the black and blue lines indicate layers 1 and 2, respectively; (c) The corresponding 2D crease pattern of layer 1; (d) The corresponding 2D crease pattern of layer 2; (e) The  $\theta_s$  versus  $\theta_b$  curve where the blue circle indicates the designed state.

### **List of tables**

Table 1	The calculated parameters of the first example.
Table 2	The calculated parameters of the second example
Table 3	The calculated parameters of the first developable and flat-foldable ring design example.
Table 4	The calculated parameters of the second developable and flat-foldable ring design example.
Table 5	The calculated parameters of layer 1 of the stacked ring design example.
Table 6	The calculated parameters of layer 2 of the stacked ring design example.

### **List of attached electronic supplementary material**

Supplementary_material.pdf	Supplementary material, sections A, B and C
Movie S1.wmv	An animation of the folding motion of the first example.
Movie S2.wmv	An animation of the folding motion of the second example.
Movie S3.wmv	An animation of the folding motion of the first ring design example.
Movie S4.wmv	An animation of the folding motion of the second ring design example.
Movie S5.wmv	An animation of the folding motion of the stacked design example.
Movie S6.wmv	An animation of the cross-sectional profile changes of the stacked design example.
Matlab_code_fig_4_Movie_ S1.zip	MATLAB codes for figure 4 and movie S1.
Matlab_code_fig_5_Movie_ S2.zip	MATLAB codes for figure 5 and movie S2.
Matlab_code_fig_7_Movie_ S3.zip	MATLAB codes for figure 7 and movie S3.
Matlab_code_fig_8_Movie_ S4.zip	MATLAB codes for figure 8 and movie S4.
Matlab_code_fig_10_Movie_ _S5&S6.zip	MATLAB codes for figure 10 and movies S5 and S6.

Figure 1

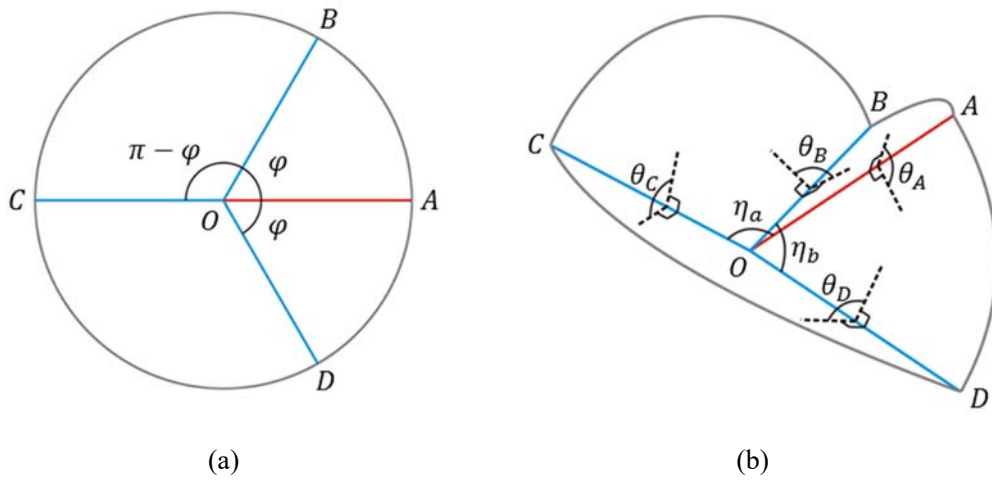
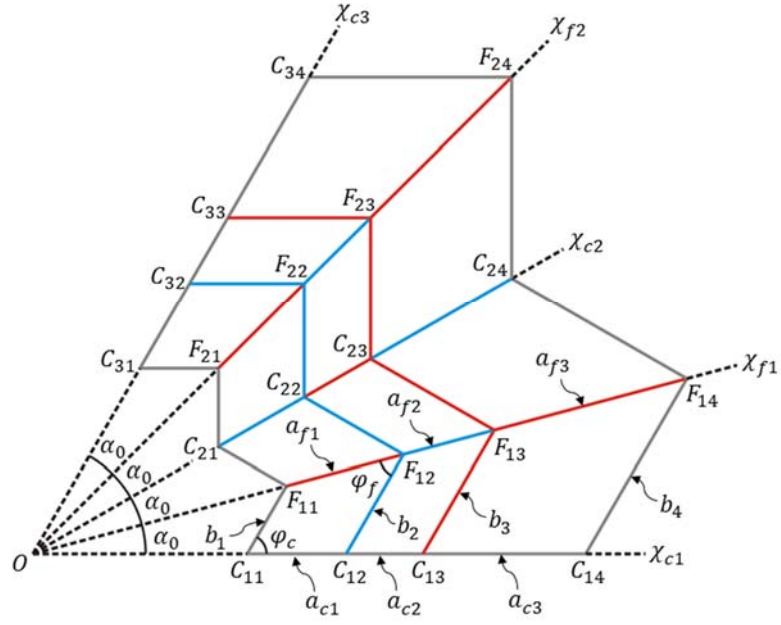
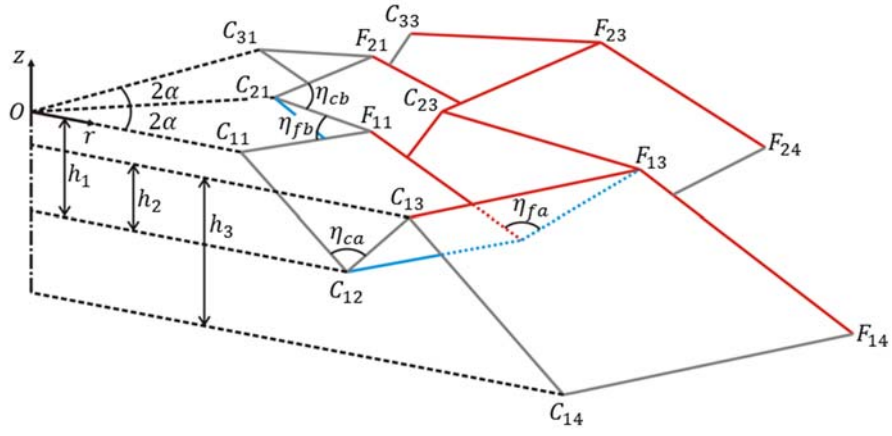


Figure 2



(a)



(b)

Figure 3

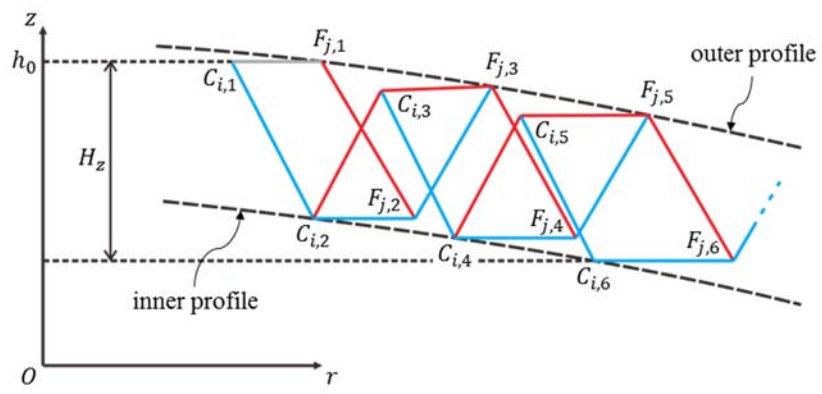
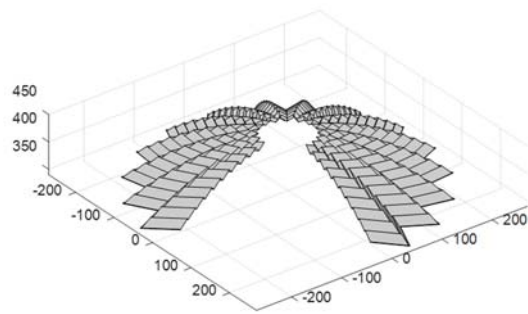
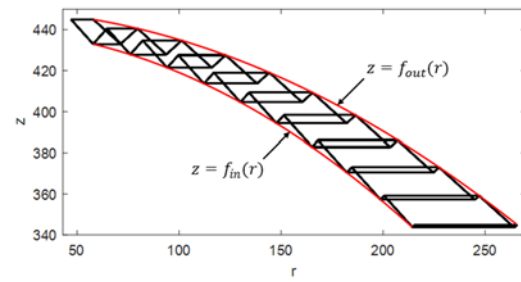




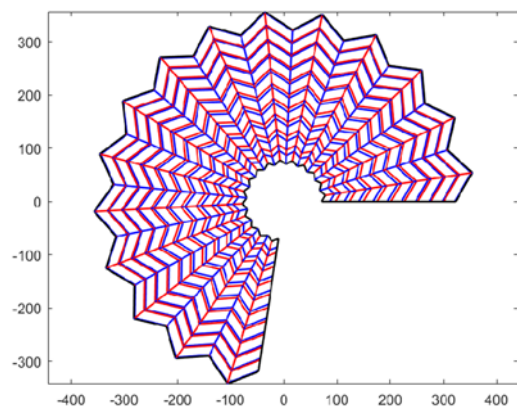
Figure 4



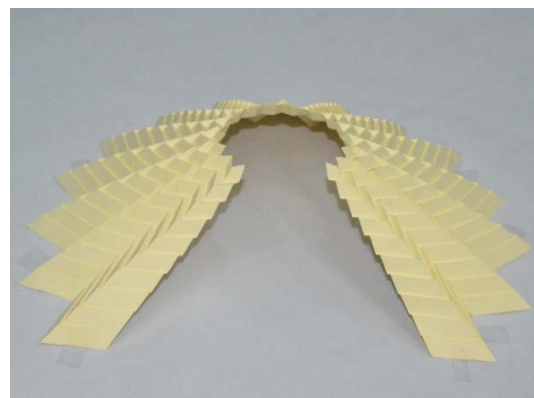
(a)



(b)

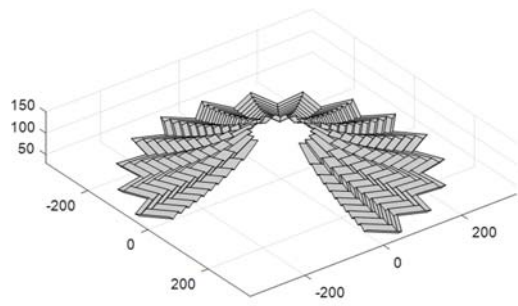


(c)

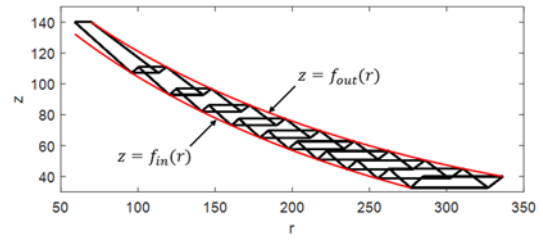


(d)

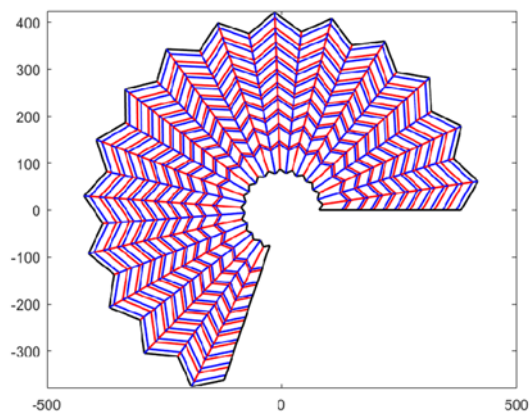
Figure 5



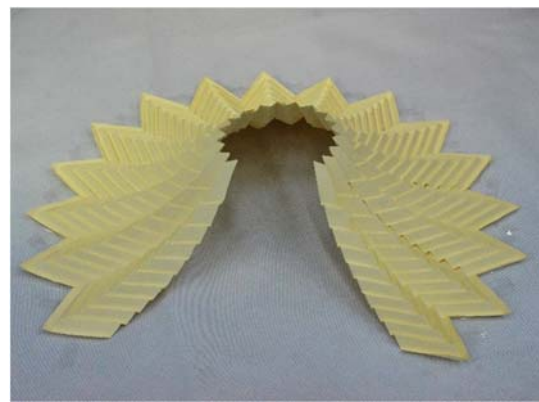
(a)



(b)



(c)



(d)

Figure 6

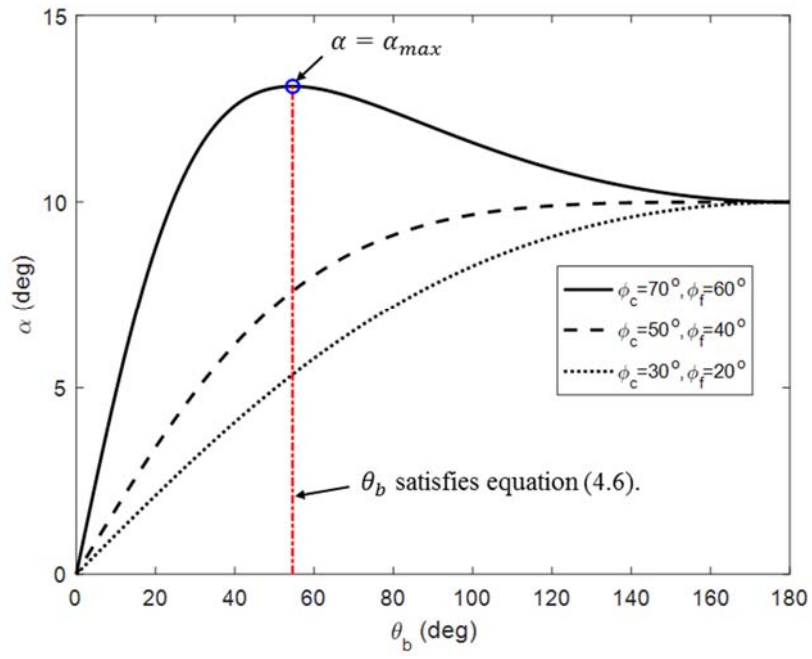
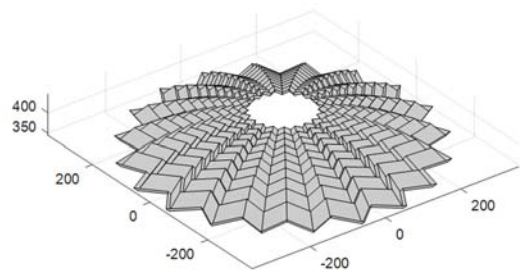
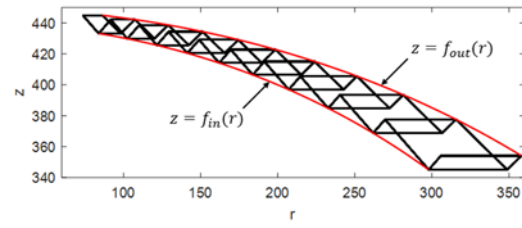


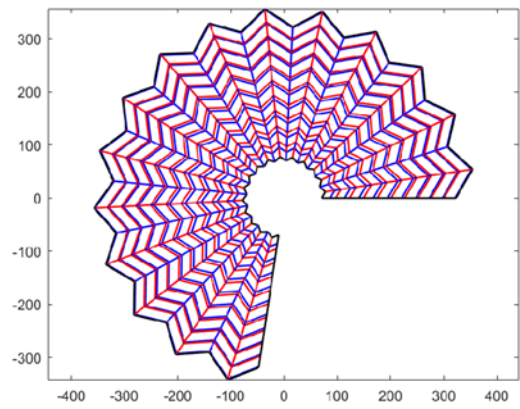
Figure 7



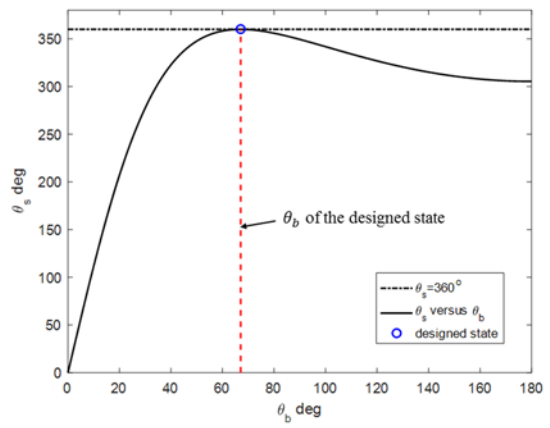
(a)



(b)



(c)

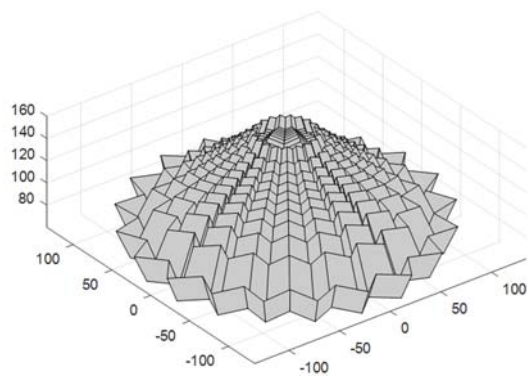


(d)

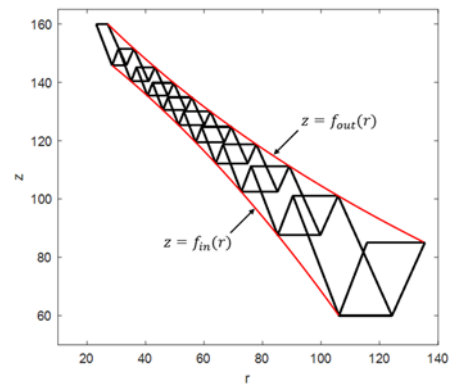


(e)

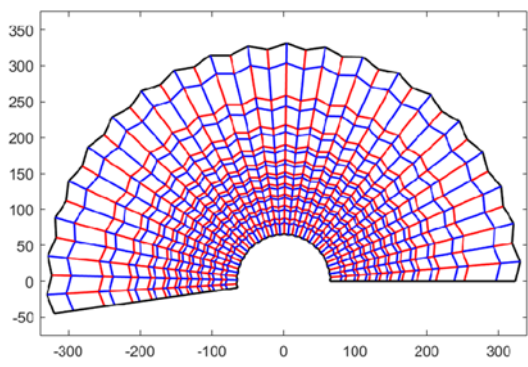
Figure 8



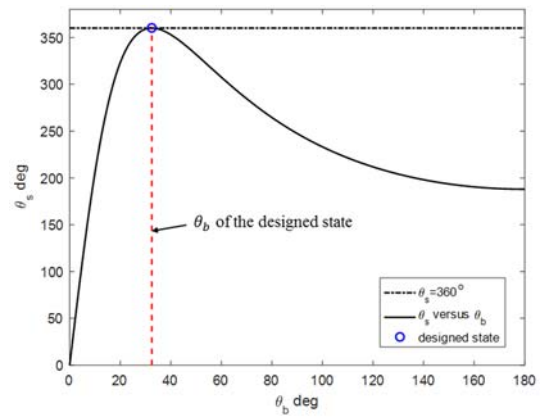
(a)



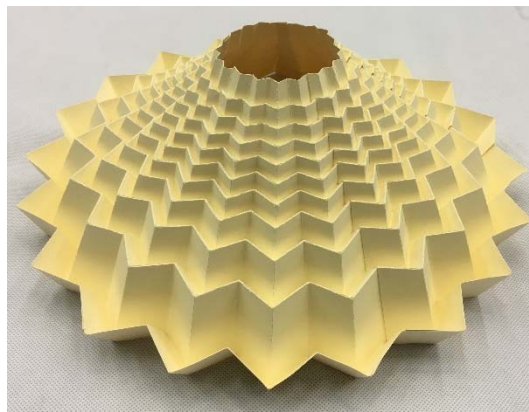
(b)



(c)



(d)



(e)

Figure 9

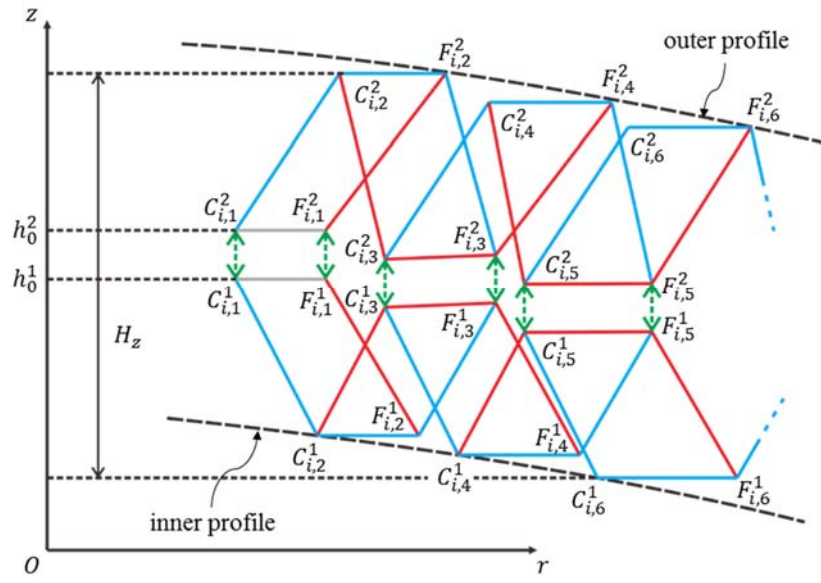
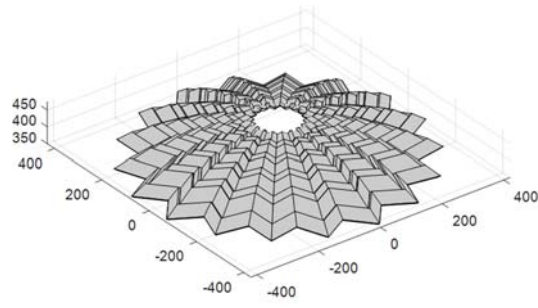
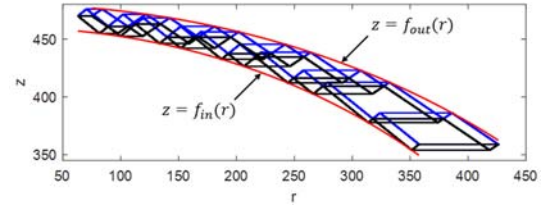


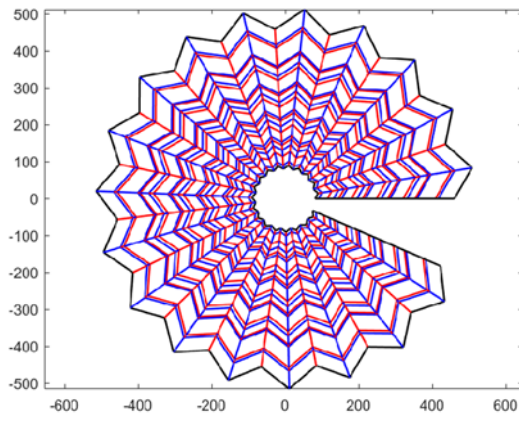
Figure 10



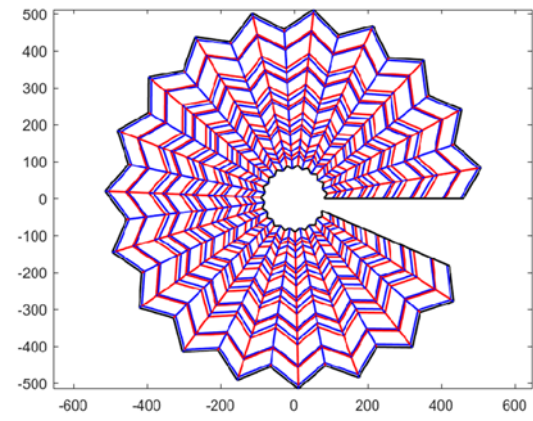
(a)



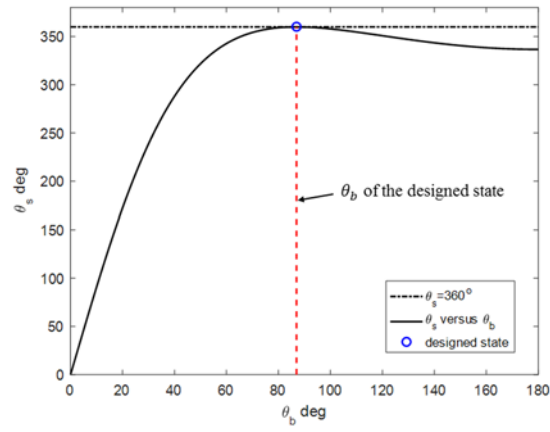
(b)



(c)



(d)



(e)

Figure S1

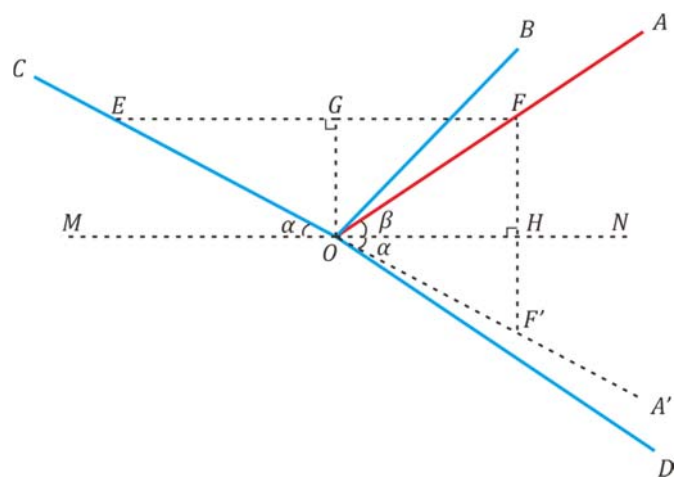




Figure S2

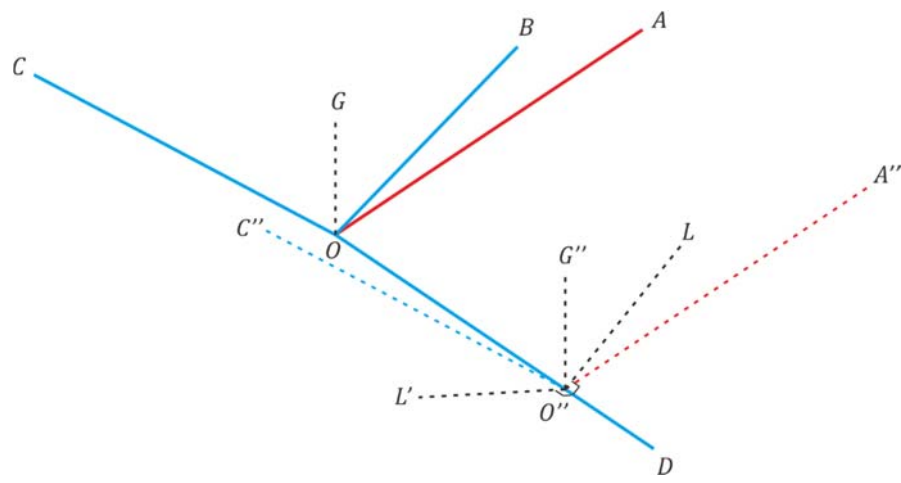


Figure S3

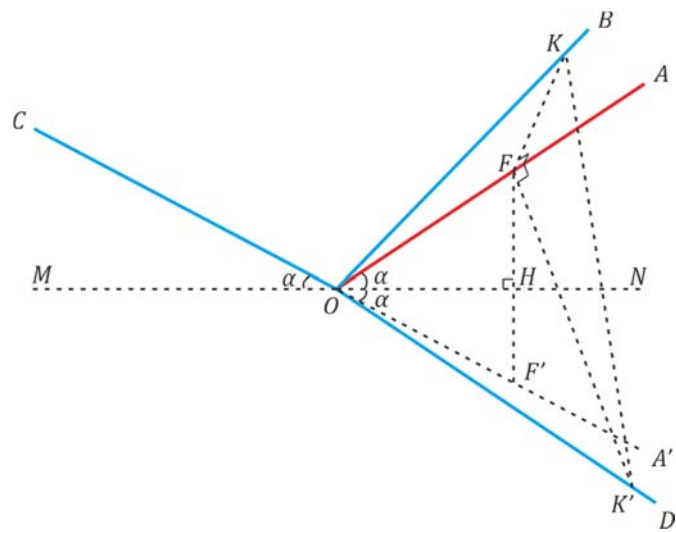


Table 1

Parameter	Value	Parameter	Value	Parameter	Value
$\alpha$	$\pi/20$ rad	$a_{c1}$	16.143 mm	$a_{c11}$	20.160 mm
$\varphi_f$	0.895 rad	$a_{c2}$	10.175 mm	$a_{c12}$	5.361 mm
$\theta_{ca}$	1.746 rad	$a_{c3}$	17.031 mm	$a_{c13}$	20.733 mm
$\theta_{fa}$	1.523 rad	$a_{c4}$	9.208 mm	$a_{c14}$	4.418 mm
$\theta_b$	1.076 rad	$a_{c5}$	17.889 mm	$a_{c15}$	21.128 mm
$\eta_{ca}$	1.464 rad	$a_{c6}$	8.241 mm	$a_{c16}$	3.493 mm
$\eta_{cb}$	1.451 rad	$a_{c7}$	18.708 mm	$a_{c17}$	21.227 mm
$\eta_{fa}$	1.673 rad	$a_{c8}$	7.276 mm	$a_{c18}$	2.597 mm
$\eta_{fb}$	1.137 rad	$a_{c9}$	19.473 mm	$a_{c19}$	20.789 mm
$b_1$	13.665 mm	$a_{c10}$	6.315 mm	$a_{c20}$	1.747 mm

Table 2

Parameter	Value	Parameter	Value	Parameter	Value
$\alpha$	$\pi/20$ rad	$a_{c1}$	49.445 mm	$a_{c11}$	17.827 mm
$\varphi_f$	0.901 rad	$a_{c2}$	5.833 mm	$a_{c12}$	7.440 mm
$\theta_{ca}$	2.056 rad	$a_{c3}$	27.089 mm	$a_{c13}$	17.602 mm
$\theta_{fa}$	1.856 rad	$a_{c4}$	5.929 mm	$a_{c14}$	8.078 mm
$\theta_b$	1.385 rad	$a_{c5}$	22.030 mm	$a_{c15}$	17.677 mm
$\eta_{ca}$	1.682 rad	$a_{c6}$	6.159 mm	$a_{c16}$	8.847 mm
$\eta_{cb}$	1.671 rad	$a_{c7}$	19.685 mm	$a_{c17}$	18.004 mm
$\eta_{fa}$	1.846 rad	$a_{c8}$	6.490 mm	$a_{c18}$	9.778 mm
$\eta_{fb}$	1.357 rad	$a_{c9}$	18.452 mm	$a_{c19}$	18.566 mm
$b_1$	14.719 mm	$a_{c10}$	6.915 mm	$a_{c20}$	10.910 mm

Table 3

Parameter	Value	Parameter	Value	Parameter	Value
$\alpha$	$\pi/20$ rad	$a_{c1}$	15.615 mm	$a_{c11}$	21.695 mm
$\varphi_f$	0.997 rad	$a_{c2}$	11.924 mm	$a_{c12}$	11.435 mm
$\theta_{ca}$	1.997 rad	$a_{c3}$	16.403 mm	$a_{c13}$	24.095 mm
$\theta_{fa}$	1.768 rad	$a_{c4}$	11.761 mm	$a_{c14}$	11.450 mm
$\theta_b$	1.170 rad	$a_{c5}$	17.343 mm	$a_{c15}$	27.495 mm
$\eta_{ca}$	1.433 rad	$a_{c6}$	11.629 mm	$a_{c16}$	11.521 mm
$\eta_{cb}$	1.728 rad	$a_{c7}$	18.482 mm	$a_{c17}$	32.838 mm
$\eta_{fa}$	1.591 rad	$a_{c8}$	11.530 mm	$a_{c18}$	11.675 mm
$\eta_{fb}$	1.414 rad	$a_{c9}$	19.893 mm	$a_{c19}$	43.161 mm
$b_1$	17.738 mm	$a_{c10}$	11.464 mm	$a_{c20}$	11.982 mm

Table 4

Parameter	Value	Parameter	Value	Parameter	Value
$\alpha$	$\pi/20$ rad	$a_{c1}$	15.215 mm	$a_{c11}$	11.286 mm
$\varphi_f$	1.254 rad	$a_{c2}$	6.164 mm	$a_{c12}$	5.687 mm
$\theta_{ca}$	1.795 rad	$a_{c3}$	12.009 mm	$a_{c13}$	13.410 mm
$\theta_{fa}$	1.505 rad	$a_{c4}$	5.193 mm	$a_{c14}$	6.998 mm
$\theta_b$	0.567 rad	$a_{c5}$	10.521 mm	$a_{c15}$	17.420 mm
$\eta_{ca}$	0.732 rad	$a_{c6}$	4.768 mm	$a_{c16}$	9.456 mm
$\eta_{cb}$	1.728 rad	$a_{c7}$	10.011 mm	$a_{c17}$	25.392 mm
$\eta_{fa}$	0.844 rad	$a_{c8}$	4.714 mm	$a_{c18}$	14.464 mm
$\eta_{fb}$	1.414 rad	$a_{c9}$	10.254 mm	$a_{c19}$	44.019 mm
$b_1$	5.560 mm	$a_{c10}$	4.997 mm	$a_{c20}$	26.790 mm

Table 5

Parameter	Value	Parameter	Value	Parameter	Value
$\alpha^1$	$\pi/18$ rad	$a_{c1}^1$	23.519 mm	$a_{c11}^1$	17.790 mm
$\varphi_f^1$	0.884 rad	$a_{c2}^1$	9.870 mm	$a_{c12}^1$	12.922 mm
$\theta_{ca}^1$	2.171 rad	$a_{c3}^1$	13.869 mm	$a_{c13}^1$	34.827 mm
$\theta_{fa}^1$	1.963 rad	$a_{c4}^1$	16.682 mm	$a_{c14}^1$	6.678 mm
$\theta_b^1$	1.518 rad	$a_{c5}^1$	26.082 mm	$a_{c15}^1$	22.041 mm
$\eta_{ca}^1$	1.783 rad	$a_{c6}^1$	8.843 mm	$a_{c16}^1$	10.810 mm
$\eta_{cb}^1$	1.745 rad	$a_{c7}^1$	15.488 mm	$a_{c17}^1$	48.055 mm
$\eta_{fa}^1$	1.950 rad	$a_{c8}^1$	14.839 mm	$a_{c18}^1$	5.385 mm
$\eta_{fb}^1$	1.396 rad	$a_{c9}^1$	29.460 mm	$a_{c19}^1$	41.048 mm
$b_1^1$	16.422 mm	$a_{c10}^1$	7.795 mm	$a_{c20}^1$	8.089 mm

Table 6

Parameter	Value	Parameter	Value	Parameter	Value
$\alpha^2$	$\pi/18$ rad	$a_{c1}^2$	9.870 mm	$a_{c11}^2$	12.922 mm
$h_0^2$	470 mm	$a_{c2}^2$	23.519 mm	$a_{c12}^2$	17.790 mm
$\varphi_c^2$	$\pi/3$ rad	$a_{c3}^2$	16.682 mm	$a_{c13}^2$	6.678 mm
$\varphi_f^2$	0.884 rad	$a_{c4}^2$	13.869 mm	$a_{c14}^2$	34.827 mm
$\theta_{ca}^2$	2.171 rad	$a_{c5}^2$	8.843 mm	$a_{c15}^2$	10.810 mm
$\theta_{fa}^2$	1.963 rad	$a_{c6}^2$	26.082 mm	$a_{c16}^2$	22.041 mm
$\theta_b^2$	1.518 rad	$a_{c7}^2$	14.839 mm	$a_{c17}^2$	5.385 mm
$\eta_{ca}^2$	1.783 rad	$a_{c8}^2$	15.488 mm	$a_{c18}^2$	48.055 mm
$\eta_{cb}^2$	1.745 rad	$a_{c9}^2$	7.795 mm	$a_{c19}^2$	8.089 mm
$\eta_{fa}^2$	1.950 rad	$a_{c10}^2$	29.460 mm	$a_{c20}^2$	41.048 mm
$\eta_{fb}^2$	1.396 rad				
$b_1^2$	16.422 mm				



# SUPPLEMENTARY MATERIAL FOR

## Design of Rigid-foldable Doubly-Curved Origami Tessellations Based on Trapezoidal Crease Patterns

Keyao Song<sup>1</sup>, Xiang Zhou<sup>1\*</sup>, Shixi Zang<sup>1</sup>, Hai Wang<sup>1</sup>, Zhong You<sup>2</sup>

<sup>1</sup> School of Aeronautics and Astronautics, Shanghai Jiao Tong University, No. 800 Dongchuan  
Road, Shanghai, 200240, China

<sup>2</sup> Department of Engineering Science, University of Oxford, Parks Road, Oxford, OX3 0PL, UK

### A. Folding kinematics of a single degree-4 vertex

Equation (2.2) holds and plane  $AOC$  is perpendicular to plane  $BOD$  due to symmetry.

Refer now to figure S1, where planes  $AOC$  and  $BOD$  intersect at line  $MN$ ,  $OA'$  and  $OC$  are collinear,  $|OE| = |OF|$ ,  $OG \perp EF$ , and  $FF'$  is perpendicular to  $MN$  and intersects  $MN$  at  $H$ . Because plane  $AON$  is perpendicular to plane  $NOD$ , applying the cosine law respectively to  $\angle AON$ ,  $\angle DON$  and  $\angle AOD$  leads to the following relationship.

$$\cos \angle AON \cos \angle DON = \cos \angle AOD. \quad (A1)$$

Similarly, there is

$$\cos \angle A'ON \cos \angle DON = \cos \angle A'OD. \quad (A2)$$

Because  $\angle AOD = \varphi$  and  $\angle A'OD = \pi - \angle COD = \varphi$ , combining equations (A1) and (A2) yields  $\angle AON = \angle A'ON$ . Considering that  $\angle AOC = \eta_a$ , we get

$$\angle AON = \angle A'ON = \frac{\pi - \eta_a}{2}. \quad (A3)$$

Due to symmetry, there is

$$\angle DON = \frac{\angle BOD}{2} = \frac{\eta_b}{2}. \quad (A4)$$

Substituting equations (A3) and (A4) and  $\angle AOD = \varphi$  into equation (A1) yields

---

\* Corresponding author, e-mail: xiangzhou@sjtu.edu.cn, telephone: +86 21 34207538, corresponding address: School of Aeronautics and Astronautics, No. 800 Dongchuan Road, Shanghai, 200240, China.

$$\cos\left(\frac{\pi}{2} - \frac{\eta_a}{2}\right) \cos\left(\frac{\eta_b}{2}\right) = \cos \varphi. \quad (\text{A5})$$

Applying the double angle formula to equation (A5) yields

$$(1 + \cos \eta_b)(1 - \cos \eta_a) = 4\cos^2 \varphi. \quad (\text{A6})$$

In isosceles triangle  $\triangle EOF$ , because  $OG \perp EF$ ,  $OG$  is also the bisector of  $\angle EOF$ . Because  $\angle A'ON = \angle COM$ , we get  $\angle COM = \angle AON$  according to equation (A3). Therefore,  $OG$  is perpendicular to  $MN$ . Because  $MN$  is the intersection line of two perpendicular planes  $AOC$  and  $BOD$  and  $OG$  is in plane  $AOC$ ,  $OG$  is perpendicular to plane  $BOD$ .

Refer now to figure S2, where  $O''C'' \parallel OC$ ,  $O''G'' \parallel OG$ ,  $O''A'' \parallel OA$ ,  $O''L$  is in plane  $AOC$  and perpendicular to  $OD$  and  $O''L'$  is in plane  $COD$  and perpendicular to  $OD$ . According to the definition of  $\theta_B$ ,  $\angle LO''L' = \theta_B$ . Because  $OG$  is perpendicular to plane  $BOD$ ,  $OG$  is perpendicular to  $OD$  which is in plane  $BOD$ . Because  $O''G'' \parallel OG$ , we get  $O''G'' \perp OD$ . Because  $O''L \perp OD$  and  $O''G'' \perp OD$ ,  $OD$  is perpendicular to plane  $G''O''L$  and hence plane  $AOD$  is perpendicular to plane  $G''O''L$ . Applying the cosine law respectively to  $\angle A''O''L$ ,  $\angle LO''G''$  and  $\angle A''O''G''$  leads to the following relationship.

$$\cos \angle A''O''L \cos \angle LO''G'' = \cos \angle A''O''G''. \quad (\text{A7})$$

Similarly, there is

$$\cos \angle L'O''G'' \cos \angle C''O''L' = \cos \angle C''O''G''. \quad (\text{A8})$$

Because  $O''G''$  bisectors  $\angle A''O''C''$ ,  $\angle A''O''G'' = \angle C''O''G'' = \frac{\eta_a}{2}$ . Because  $\angle A''O''L = \angle C''O''L' = \frac{\pi}{2} - \varphi$ , combining equations (A7) and (A8) yields

$$\angle LO''G'' = \angle L'O''G'' = \frac{\angle LO''L'}{2} = \frac{\theta_B}{2}. \quad (\text{A9})$$

Substituting equation (A9) into equation (A7) yields

$$\cos\left(\frac{\pi}{2} - \frac{\varphi}{2}\right) \cdot \cos \frac{\theta_B}{2} = \cos \frac{\eta_a}{2}. \quad (\text{A10})$$

Applying the double angle formula to both sides of equation (A10) gives equation (2.4).

Refer now to figure S3, where both  $FK$  and  $FK'$  are perpendicular to  $OA$ , and  $FF'$  is perpendicular to  $MN$  and intersects  $MN$  at  $H$ . According to the definition of  $\theta_A$ ,  $\angle KFK' = \theta_A$ .

In isosceles triangle  $\triangle KFK'$ , according to the cosine law, there is

$$|K'F|^2 + |KF|^2 - |K'K|^2 = 2|K'F| \cdot |KF| \cos \angle KFK'. \quad (\text{A11})$$

Similarly, in isosceles triangle  $\Delta KOK'$ , there is

$$|K'O|^2 + |KO|^2 - |K'K|^2 = 2|K'O| \cdot |KO| \cos \angle KOK'. \quad (\text{A12})$$

In right triangle  $\Delta OFK$ , there is

$$\sin \angle KOF = \frac{|KF|}{|KO|}. \quad (\text{A13})$$

Similarly, in right triangle  $\Delta OFK'$ , there is

$$\sin \angle K'OF = \frac{|K'F|}{|K'O|}. \quad (\text{A14})$$

Combining equations (A11) to (A14) and considering  $|KF| = |K'F|$ ,  $|KO| = |K'O|$ ,  $\angle KFK' = \theta_A$ ,  $\angle KOK' = \eta_b$  and  $\angle KOF = \angle K'OF = \varphi$ , we get equation (2.5). By substituting equations (2.4) and (2.5) into equation (A6), equation (2.3) can be obtained. Finally, imaging that we connect points  $F'$  and  $K$  and points  $F'$  and  $K'$  in figure S3, there are  $F'K \perp OA'$ ,  $F'G' \perp OA'$  and  $|KF'| = |K'F'|$  due to symmetry. Hence,  $\angle KF'K' = \theta_c$ . Using the similar procedure for equation (2.5), the following relationship can be derived.

$$\cos \eta_b = \sin^2 \varphi \cos \theta_c + \cos^2 \varphi. \quad (\text{A15})$$

Combining equations (2.5) and (A15), we get equation (2.1).

## B. The developable and flat-foldable conditions for the ring design

Substituting equations (2.12) and (2.14) into equations (2.9) and (2.10), respectively, yields

$$\eta_{cb} = \cos^{-1} \left( \frac{4 \cos^2 \varphi_c}{1 + \cos^2 \varphi_c - \sin^2 \varphi_c \cos \theta_b} - 1 \right), \quad (\text{B1})$$

$$\eta_{fb} = \cos^{-1} \left( \frac{4 \cos^2 \varphi_f}{1 + \cos^2 \varphi_f - \sin^2 \varphi_f \cos \theta_b} - 1 \right). \quad (\text{B2})$$

Substituting equations (B1) and (B2) into equation (2.16) yields

$$\alpha = \frac{1}{2} \left( \cos^{-1} \left( \frac{4 \cos^2 \varphi_c}{1 + \cos^2 \varphi_c - \sin^2 \varphi_c \cos \theta_b} - 1 \right) - \cos^{-1} \left( \frac{4 \cos^2 \varphi_f}{1 + \cos^2 \varphi_f - \sin^2 \varphi_f \cos \theta_b} - 1 \right) \right). \quad (\text{B3})$$

Equation (B3) gives the relationship between  $\alpha$  and  $\theta_b$ . In order for a folded structure to be developable and flat-foldable,  $\theta_s$  of the folded structure at any interim state cannot exceed  $2\pi$ .

Because  $\theta_s$  at the designed state, denoted by  $\bar{\theta}_s$ , equals  $2\pi$ , the following relationship holds

$$\theta_s \leq \bar{\theta}_s. \quad (\text{B4})$$

Denote  $\alpha$  at the designed state by  $\bar{\alpha}$ . Substituting equation (2.28) into inequality (B4) yields

$$\alpha \leq \bar{\alpha}. \quad (\text{B5})$$

Inequality (B5) indicates that in order for the designed folded ring structure to be developable and flat-foldable,  $\bar{\alpha}$  should be the maximum value of all  $\alpha$  values of the structure throughout folding, i.e.  $\bar{\alpha} = \alpha_{max}$ . Because  $\alpha$  is a function of  $\theta_b$  according to equation (B3), the value of  $\theta_b$  corresponding to  $\alpha_{max}$  can be determined as

$$\frac{d\alpha}{d\theta_b} = 0. \quad (\text{B6})$$

Substituting equation (B3) into equation (B6) yields equation (3.3). In order that a real  $\theta_b$  can be solved from equation (3.3), the following inequality needs to be satisfied.

$$\left| \frac{\sin 2\varphi_f (1 + \cos^2 \varphi_c) - \sin 2\varphi_c (1 + \cos^2 \varphi_f)}{\sin 2\varphi_f \sin^2 \varphi_c - \sin 2\varphi_c \sin^2 \varphi_f} \right| \leq 1. \quad (\text{B8})$$

As the designed state can be neither the 2D crease pattern (i.e.  $\theta_b = \pi$ ) nor the fully folded state (i.e.  $\theta_b = 0$ ), the equal sign needs to be removed from inequality (B8), which leads to

$$\cos \varphi_f \cos \varphi_c \sin(\varphi_c - \varphi_f) > 0, \quad (\text{B9})$$

$$\sin 2\varphi_f > \sin 2\varphi_c. \quad (\text{B10})$$

Because of equation (2.6), inequality (B9) always holds. Considering equation (2.6) and inequality (B10), we obtain inequality (3.2).

### C. The compatible folding condition for the stacked design

According to equations (2.16), there is

$$\begin{aligned} \cos \alpha &= \cos \left( \frac{\eta_{cb}}{2} - \frac{\eta_{fb}}{2} \right) \\ &= \sqrt{\frac{1 + \cos \eta_{cb}}{2}} \sqrt{\frac{1 + \cos \eta_{fb}}{2}} + \sqrt{\frac{1 - \cos \eta_{cb}}{2}} \sqrt{\frac{1 - \cos \eta_{fb}}{2}}. \end{aligned} \quad (\text{C1})$$

Substituting equations (2.9) to (2.14) into equation (C1) yields

$$\begin{aligned} \cos \alpha &= \left( 2 \cos \varphi_c \cos \varphi_f + \sin \varphi_c \sin \varphi_f (1 - \cos \theta_b) \right) \\ &\cdot \sqrt{\frac{1}{(1 + \cos^2 \varphi_c - \sin^2 \varphi_c \cos \theta_b)(1 + \cos^2 \varphi_f - \sin^2 \varphi_f \cos \theta_b)}}. \end{aligned} \quad (\text{C2})$$

The  $z$ -directional height between any two C-type vertices  $C_{i,p}$  and  $C_{i,q}$  and any two F-type vertices  $F_{i,p}$  and  $F_{i,q}$  can be expressed as

$$h_z^c = - \sum_{k=p}^q a_{c,k} (-1)^k \cos \frac{\eta_{ca}}{2} = H_c \cos \frac{\eta_{ca}}{2}, \quad (C3)$$

$$h_z^f = - \sum_{k=p}^q a_{f,k} (-1)^k \cos \frac{\eta_{fa}}{2} = H_f \cos \frac{\eta_{fa}}{2}, \quad (C4)$$

respectively, where  $H_c = - \sum_{k=p}^q a_{c,k} (-1)^k$  and  $H_f = - \sum_{k=p}^q a_{f,k} (-1)^k$ . Considering equation (2.23), there is  $h_z^c = h_z^f$ . Hence, we use  $h_z$  to denote both  $h_z^c$  and  $h_z^f$  in the sequel. Applying the double angle formula to equations (C3) and (C4) yields

$$h_z = H_c \sqrt{\frac{(1 + \cos \eta_{ca})}{2}}, \quad (C5)$$

$$h_z = H_f \sqrt{\frac{(1 + \cos \eta_{fa})}{2}}. \quad (C6)$$

Substituting equations (2.11) and (2.13) into equations (C5) and (C6), respectively, yields

$$h_z = H_c \sqrt{\frac{(1 + \cos \theta_b) \cdot \sin^2 \varphi_c}{2}} \quad (C5)$$

$$h_z = H_f \sqrt{\frac{(1 + \cos \theta_b) \cdot \sin^2 \varphi_f}{2}}. \quad (C6)$$

Combining equations (C2), (C5) and (C6) to eliminate  $\cos \theta_b$  yields

$$\begin{aligned} \cos \alpha = & \left( \cos \varphi_c \cos \varphi_f + \sin \varphi_c \sin \varphi_f \left( 1 - \frac{h_z^2}{\sin^2 \varphi_c \cdot H_c^2} \right) \right) \\ & \cdot H_c H_f \sqrt{\frac{1}{(H_c^2 - h_z^2)(H_f^2 - h_z^2)}}. \end{aligned} \quad (C7)$$

Consider now a stacked design consisting of two folded layers. In order for the two layers to fold in a compatible mode, the sufficient and necessary condition is that when  $\alpha^1 = \alpha^2 = \alpha$ , the constraints on the interface between the two layers are always satisfied. In the  $z$  direction, the constraint can be equivalently given as  $h_z^1 = h_z^2 = h_z$ , which, by considering equation (C7), can be expressed as

$$\begin{aligned}
& \left( \cos \varphi_c^1 \cos \varphi_f^1 + \sin \varphi_c^1 \sin \varphi_f^1 \left( 1 - \frac{h_z^2}{\sin^2 \varphi_c^1 \cdot (H_c^1)^2} \right) \right) \\
& \cdot H_c^1 H_f^1 \sqrt{\frac{1}{((H_c^1)^2 - h_z^2)((H_f^1)^2 - h_z^2)}} \\
& - \left( \cos \varphi_c^2 \cos \varphi_f^2 + \sin \varphi_c^2 \sin \varphi_f^2 \left( 1 - \frac{h_z^2}{\sin^2 \varphi_c^2 \cdot (H_c^2)^2} \right) \right) \\
& \cdot H_c^2 H_f^2 \sqrt{\frac{1}{((H_c^2)^2 - h_z^2)((H_f^2)^2 - h_z^2)}} \equiv 0.
\end{aligned} \tag{C8}$$

Since equation (C8) holds for arbitrary  $h_z$ , the following relationships can be obtained.

$$\cos(\varphi_c^1 - \varphi_f^1) = \cos(\varphi_c^2 - \varphi_f^2), \tag{C9}$$

$$H_c^1 = H_c^2, \tag{C10}$$

$$H_f^1 = H_f^2. \tag{C11}$$

Substituting equations (2.7),  $H_c = -\sum_{k=p}^q a_{c,k}(-1)^k$  and  $H_f = -\sum_{k=p}^q a_{f,k}(-1)^k$  into equations (C10) and (C11) yields

$$\frac{\sin \varphi_c^1}{\sin \varphi_f^1} = \frac{\sin \varphi_c^2}{\sin \varphi_f^2}. \tag{C12}$$

Combining equation (C9) and (C12) yields

$$\varphi_f^1 = \varphi_f^2, \tag{C13}$$

$$\varphi_c^1 = \varphi_c^2. \tag{C14}$$

It should be pointed out that equations (C13) and (C14) are dependent. Given that  $\varphi_c^1 = \varphi_c^2$ , combining equations (C14), (2.9), (2.12) and (3.13) yields

$$\theta_b^1 = \theta_b^2. \tag{C16}$$

Then, by combining equations (C16), (C14) and (C2), equation (C13) can be obtained.

It is further noted that with equation (C14), the constraint in the  $r$  direction is satisfied as well. This can be proved as follow. By substituting equations (C14) and (C16) into equation (2.11), we get

$$\eta_{ca}^1 = \eta_{ca}^2. \tag{C17}$$

Substituting equations (C13) and (C16) into equation (3.13) gives

$$\eta_{fa}^1 = \eta_{fa}^2. \tag{C18}$$

Finally, by combining equations (C10), (C11), (C17), (C18) and (3.13), equation (3.16) can be

obtained.

In summary, equation (C14) is the sole compatible folding condition for the stacked design.

Figure S1

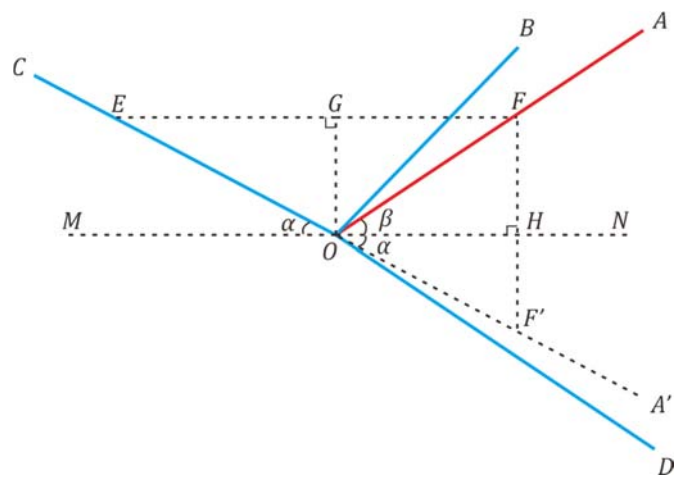




Figure S2

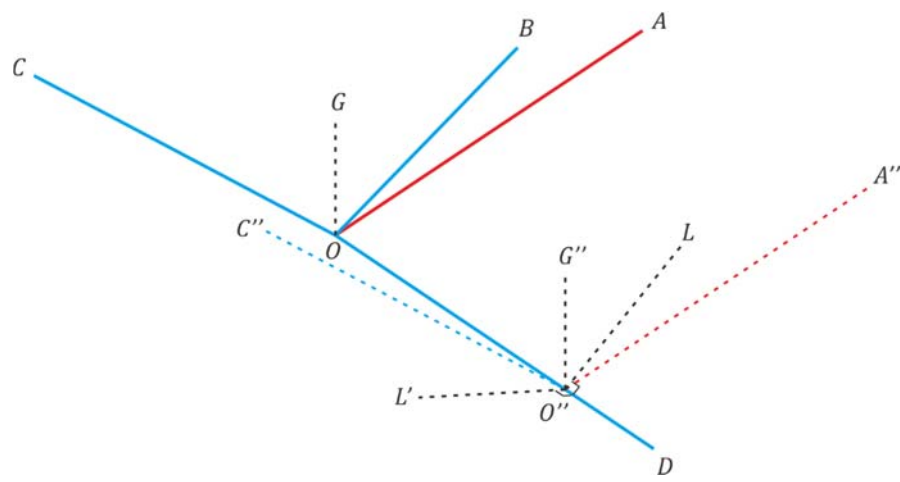


Figure S3

